

Article

Enhancing Carbon Fiber Fabrics with ALD Al_xO_y Coatings: An Investigation of Thickness Effects on Weight, Morphology, Coloration, and Thermal Properties

Vanessa Dias ¹, Nierlly Galvão ², Felipe Miranda ¹ , Mariana Fraga ³, Gilberto Petraconi ¹, Homero Maciel ¹ and Rodrigo Pessoa ^{1,*} 

¹ Plasmas and Processes Laboratory, Aeronautics Institute of Technology (ITA), São José dos Campos 12228-900, Brazil; vannyummy@gmail.com (V.D.); mirannnda.fs@gmail.com (F.M.); gilberto@ita.br (G.P.); homero@ita.br (H.M.)

² School of Engineering, Mackenzie Presbyterian University, São Paulo 01221-040, Brazil; nierlly@gmail.com

³ Associate Laboratory of Sensors and Materials, National Institute for Space Research (INPE), São José dos Campos 12227-010, Brazil; mariana.fraga@mackenzie.br

* Correspondence: rspessoa@ita.br; Tel.: +55-12-3947-5875

Abstract: This study explores the impact of non-stoichiometric aluminum oxide (Al_xO_y) coatings applied via thermal atomic layer deposition (ALD) on carbon fiber fabrics (CFFs), emphasizing volume per cycle, FESEM analyses, color transitions, and thermal stability enhancements. Using trimethylaluminum and water at 100 °C, Al_xO_y was deposited across a range of 1000 to 5000 ALD cycles, with film thicknesses extending up to 500 nm. This notable increase in the volume of material deposited per cycle was observed for the 3D CFFs, highlighting ALD's capability to coat complex structures effectively. FESEM analyses revealed the morphological evolution of CFF surfaces post-coating, showing a transition from individual grains to a dense, continuous layer as ALD cycles increased. This morphological transformation led to significant color shifts from green to red to blue, attributed to structural coloration effects arising from variations in film thickness and surface morphology. Thermogravimetric analyses (TGA and dTG) indicated that the Al_xO_y coatings enhanced the thermal stability of CFFs, with a postponement in degradation onset observed in samples subjected to more ALD cycles. In essence, this research highlights the nuanced relationship between ALD processing parameters and their collective influence on both the aesthetic and functional properties of CFFs. This study illustrates ALD's potential in customizing CFFs for applications requiring specific color and thermal resilience, balancing the discussion between the surface morphological changes and their implications for color and thermal behavior.

Keywords: carbon fiber fabrics; atomic layer deposition; alumina; DataColor spectrophotometry; thermal resistance



Citation: Dias, V.; Galvão, N.; Miranda, F.; Fraga, M.; Petraconi, G.; Maciel, H.; Pessoa, R. Enhancing Carbon Fiber Fabrics with ALD Al_xO_y Coatings: An Investigation of Thickness Effects on Weight, Morphology, Coloration, and Thermal Properties. *Coatings* **2024**, *14*, 596. <https://doi.org/10.3390/coatings14050596>

Received: 1 April 2024

Revised: 5 May 2024

Accepted: 8 May 2024

Published: 9 May 2024



Copyright: © 2024 by the authors. Licensee MDPI, Basel, Switzerland. This article is an open access article distributed under the terms and conditions of the Creative Commons Attribution (CC BY) license (<https://creativecommons.org/licenses/by/4.0/>).

1. Introduction

Carbon fibers (CFs), primarily composed of more than 92% carbon in a non-graphitic form, are derived from polymer-based precursors or carbon allotrope building blocks [1]. These fibers are celebrated across various industrial sectors, including aeronautics, aerospace, automotive, civil engineering, and sports, for their outstanding chemical resistance, superior tensile strength, minimal weight, low thermal conductivity, and high-temperature tolerance [2,3]. Their distinctive blend of strength, lightness, and durability renders them indispensable in high-performance applications [4,5].

Despite these attributes, CFs face a significant limitation due to their deep dark coloration resulting from their remarkable light absorption across the visible spectrum. This characteristic, stemming from their high crystallinity and chemically inert surface, makes CFs resistant to conventional coloring methods such as dyes and pigments, thereby restricting their utility in the textile industry [5,6].

Historically, the application of atomic layer deposition (ALD) on textiles, especially carbon fiber fabrics (CFFs), has proven to be a promising method to address these challenges. ALD enables the deposition of precise, conformal coatings, facilitating the functionalization of CFFs at the nanoscale [7–12]. This technique allows for the application of ultra-thin layers of materials such as aluminum oxide (Al_2O_3) and titanium dioxide (TiO_2), which impart new properties to the CFFs, including altered optical characteristics and enhanced thermal resistance [6–8]. Such modifications fundamentally transform the natural dark hue of the fibers, yielding a spectrum of vibrant and visually striking colors. Crucially, this color transformation is directly linked to the thickness of the applied metal oxide films. Variations in film thickness lead to shifts in the intensity and wavelength spectrum of the reflected light, producing a diverse palette of colors. This precise control inherent to ALD not only boosts the aesthetic appeal of CFFs but also broadens the potential for new applications where both color and material properties are essential. This aspect of the research lays the groundwork for exploring the relationships among film thickness, optical properties, and material functionality in CF-based composites.

Furthermore, ALD offers several advantages for enhancing CFFs, including the capability to chemically activate surfaces, uniformly cover high-aspect-ratio structures, and produce pinhole-free coatings. Notably, ALD achieves this with minimal weight addition to the fabrics, typically less than 1%, which is vital for maintaining the lightweight characteristics of complex substrates like CFFs [13,14]. The low-temperature growth process and the self-limiting nature of the surface reactions minimize the risk of fiber damage during the coating process. Additionally, ALD imparts significant functional attributes to the fibers, such as increased cut and heat resistance, improved hydrophobicity, and enhanced UV protection [15–19].

Previous studies have showcased the potential of ALD in transforming the intrinsic properties of CFFs. For instance, research by Chen et al. demonstrated the capability of ALD to induce vibrant, structurally colored surfaces on CFFs by manipulating the thickness of TiO_2 films. This not only enriched the aesthetic appeal of CFFs but also highlighted the technique's precision in thickness control, which is crucial for functional enhancements [16]. Similarly, Luo et al. expanded on this by developing full-color tunable and fire-retardant CFFs using an ALD strategy that employs Al_2O_3 films to achieve robust and visually appealing fibers under extreme conditions [6].

Despite these advancements, the literature reveals unresolved issues and challenges that limit the broader application of ALD on CFFs. Key among these are the optimization of film thickness for maximum thermal protection, the uniformity of film deposition over complex three-dimensional structures, and the long-term durability of the ALD coatings under operational stresses. These challenges underscore the need for continuous research to refine ALD processes and explore new material systems for CFF enhancement.

The current study builds on these foundational works by exploring the deposition of non-stoichiometric alumina (Al_xO_y) films at varying thicknesses up to 500 nm using thermal ALD. We aim to systematically evaluate how changes in film thickness influence the physical and functional properties of CFFs, such as weight, surface texture, coloration, and thermal insulation properties. By doing so, this research intends to contribute to the nuanced understanding of ALD's impact on CFFs, potentially paving the way for innovative uses of CFFs in more diverse applications.

2. Materials and Methods

2.1. Al_xO_y Coating of CFF Samples

Samples of CFFs, labeled “Carbonized Rayon Cloth—AMERITEX T-22r Echo”, were sourced from Commerce International Group Limited (Curitiba, Brazil). These fabrics exhibited a minimum carbon content of 95% and a maximum ash content of 5%, with yarn densities ranging between 1.5 and 1.6 g/cc and an average fiber diameter of 8.5 μm . Prior to deposition, the samples were cut into $4 \times 4 \text{ cm}^2$ pieces and then cleaned with nitrogen

gas to remove any particulates. For the thickness measurement studies, $4 \times 4 \text{ cm}^2$ pieces of p-type Si(100) (University Wafer Inc., South Boston, MA, USA) were also used.

To deposit Al_xO_y films, a TFS-200 ALD system from Beneq Oy (Beneq Oy, Espoo, Finland) was utilized, operating in thermal mode at $100 \text{ }^\circ\text{C}$. Trimethylaluminum (TMA, 97%, Sigma-Aldrich, São Paulo, Brazil) served as the metallic precursor, with deionized water as the oxidant. Optimal cycle time conditions, informed by a prior Al_2O_3 study [12], included a 0.15 s pulse time for TMA, a 0.75 s first purge time for N_2 , a 0.15 s pulse time for H_2O , and a 0.75 s second purge time for N_2 . Nitrogen gas (99.999%, White Martins, Jacareí, Brazil) was used as the purge gas at a 300 sccm flow rate. Precursor vapors were transferred from external reservoirs maintained at $21 \text{ }^\circ\text{C}$. The number of reaction cycles varied from 1000 to 5000 in 1000-cycle increments, with samples labeled as n- Al_xO_y /CFFs, where “n” indicates the ALD reaction cycle number.

2.2. Material Characterization

The thickness of the Al_xO_y films was measured using a KLA Tencor P-7 mechanical profilometer (KLA, Milpitas, CA, USA). To facilitate this measurement, a step was created in specific regions of the Si(100) substrates using Kapton tape. This approach was essential for determining the growth per cycle (GPC) of the film.

For the case of CFF substrates coated with Al_xO_y , the mass of the substrate was measured before and after deposition to determine the mass of the deposited film. For this purpose, an analytical balance (Quimis, model Q-500L210C, Diadema, Brazil) was used. This measurement aimed to determine the average mass gain per ALD cycle. The samples had an initial mass of the order of $1.0 \pm 0.1 \text{ g}$.

To examine the film morphology and elemental composition, Field Emission Scanning Electron Microscopy (FESEM) was conducted using a Tescan Mira instrument and software (Mita TC x64), coupled with the energy-dispersive X-ray spectroscopy (EDS) device AZtec 3.1 (Tescan Group, Kohoutovice, Czech Republic). The FESEM was operated at 10 kV, with a $200\times$ sweep interaction volume, a beam intensity of 13, a spectrum of 15, and a working distance of 15 mm.

To investigate the chemical bonds, infrared measurements were taken on an ATR-FTIR PerkinElmer 400 IR spectrometer (PerkinElmer, São Paulo, Brazil) at a resolution of 2 cm^{-1} . Each ATR spectrum was recorded with the blank ATR cell as the background.

Structural details of the films were determined through Raman spectroscopy, which was conducted using a Horiba Raman microprobe system (Horiba, São Paulo, Brazil) equipped with an Ar ion laser (532 nm) and a laser power of approximately 6 mW. The Raman spectra were recorded at room temperature over a range of 100 to 1000 cm^{-1} .

For colorimetric evaluation, the DataColor spectrophotometer 650 equipment was used, which has a wavelength range of 400 to 700 nm, along with the DataColor Tools 1.0.2 software (DataColor, Barueri, Brazil). The structural analysis of colors was conducted based on the color difference of samples with thin films according to the International Commission on Illumination (CIE) standard 1931 color scale. The incidence angle was set at 10° and four readings were taken on each sample to obtain an average value along with its standard deviation. To ensure a comprehensive assessment, three points were selected (low end, middle, and high end of the circular area) to evaluate the color uniformity effectively. All samples were positioned vertically in the equipment for standardization purposes.

Thermogravimetric analysis (TGA) was utilized to assess the thermal stability of both uncoated and ALD Al_xO_y -coated CFF. The analyses were conducted on a NETZSCH STA 449 Jupiter instrument (NETZSCH do Brasil, São Paulo, Brazil). A sample mass of 10 mg was placed in an alumina crucible and subjected to a controlled temperature increase from $25 \text{ }^\circ\text{C}$ to $900 \text{ }^\circ\text{C}$ at a heating rate of $10 \text{ }^\circ\text{C}/\text{min}$. These experiments were carried out under a synthetic air atmosphere with a constant flow rate of $50 \text{ mL}/\text{min}$ to ensure a consistent oxidative environment.

3. Results and Discussion

3.1. ALD Al_xO_y Film Growth: Comparative Analysis on Silicon and CFF Substrates

The ALD of metal oxide thin films yields varying results across different substrates, as demonstrated in our research on ALD TiO_2 [20]. This observation holds true for Al_2O_3 deposited on both planar silicon and CFFs. The growth per cycle (GPC) and resulting film volume per cycle on these substrates offer insightful contrasts due to their inherent structural differences.

Determining the GPC of ALD films on 3D substrates [21], such as CFFs, is not straightforward. Therefore, we conducted the following analysis: From Figure 1a, we determined the GPC of the alumina film deposited on a Si(100) substrate. Similarly, from Figure 1b, we calculated the average mass gain of the Al_xO_y film on the CFF substrate at a temperature of 100 °C. Based on these results, we then determined the volume of Al_xO_y per cycle for the films deposited on both substrates, as discussed in the following.

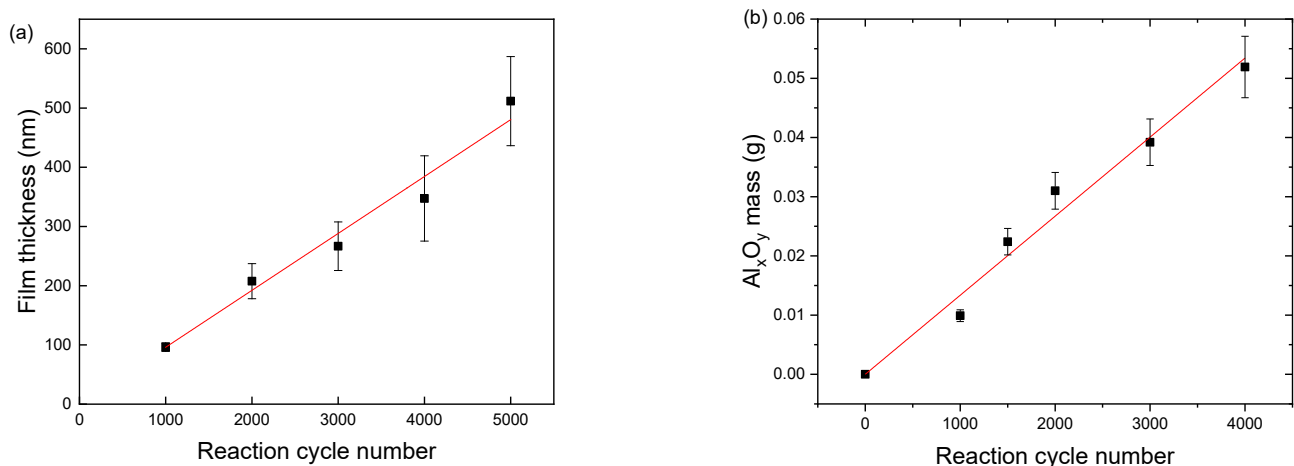


Figure 1. Al_2O_3 film growth analysis, including (a) the film thickness as a function of the number of reaction cycles on a Si(100) substrate, and (b) the mass of the Al_xO_y film post-ALD process as a function of the reaction cycles on a CFF substrate.

For the planar Si substrate, the GPC of Al_xO_y was determined to be approximately 0.096 nm/cycle. Considering a substrate area of $4 \times 4 \text{ cm}^2$, the calculated volume of Al_2O_3 deposited per cycle was approximately $1.537 \times 10^{-7} \text{ cm}^3/\text{cycle}$. This value aligns with expectations for ALD on a smooth, two-dimensional surface where the deposition is uniform and confined to the external surface area.

In contrast, our investigations on CFFs revealed a different scenario. The average mass gain per ALD cycle was found to be around $1.335 \times 10^{-5} \text{ g}/\text{cycle}$ for samples with an initial mass of approx. 1.0 g, which is equivalent to 0.0013%/cycle. Given the density of Al_2O_3 ($3.11 \text{ g}/\text{cm}^3$) [22], the calculated volume per cycle for the Al_xO_y film on CFFs was significantly higher, approximately $4.292 \times 10^{-6} \text{ cm}^3/\text{cycle}$. This stark increase in volume per cycle on CFFs can be attributed to their three-dimensional, porous structure [23], which offers a larger effective surface area for ALD deposition. The ALD process not only covers the external fibers but also permeates the internal spaces within the fabric weave [24], leading to a greater accumulation of material per cycle.

The comparison of volume per cycle values between the silicon and CFF substrates underscores the influence of substrate geometry on ALD efficiency and film growth. While the planar silicon substrate facilitates a controlled, uniform deposition, the complex architecture of CFFs enhances the deposition volume due to increased surface area and the ability of ALD to penetrate the fabric's microstructure. This penetration is further characterized by not only the typical ALD surface reactions but also additional physisorption due to the micro-porous nature of the CFF. In contrast, growth on silicon is primarily chemisorption-based, resulting in distinct film properties and growth rates. The variable nature of the

CFF surface, characterized by its fibrous and porous structure, allows for more complex interactions between the ALD precursors and the substrate, which in turn influences the kinetics of film formation. These differences highlight how substrate characteristics not only affect the physical deposition of ALD films but also significantly alter the underlying chemical dynamics of the process.

3.2. Morphological and Chemical Analysis of Al_xO_y -Coated CFF

FESEM was employed to assess the morphological characteristics of CFFs before and after the application of Al_xO_y coatings via ALD. The FESEM analysis was conducted at a range of magnifications to elucidate the alterations in the micro- and nanoscale surface features attributed to the ALD process.

The FESEM images of the uncoated CFF, as presented in Figure 2, serve as the baseline for comparison. At $100\times$ magnification (Figure 2a), the overall weave and macrostructure of the fibers were observed, providing insight into the bundling and arrangement of the individual fibers. At $10k\times$ (Figure 2b), the surface texture and uniformity of the fibers became apparent, revealing minimal impurities or variations in diameter. Increasing the magnification to $50k\times$ (Figure 2c) uncovered more intricate textural features, including morphological variations such as grains and grooves along the fibers [25,26]. The highest magnification at $100k\times$ (Figure 2d) offered a detailed microscopic view of the fiber surface, highlighting the pronounced topography and nanoscale grains along the CF surface.

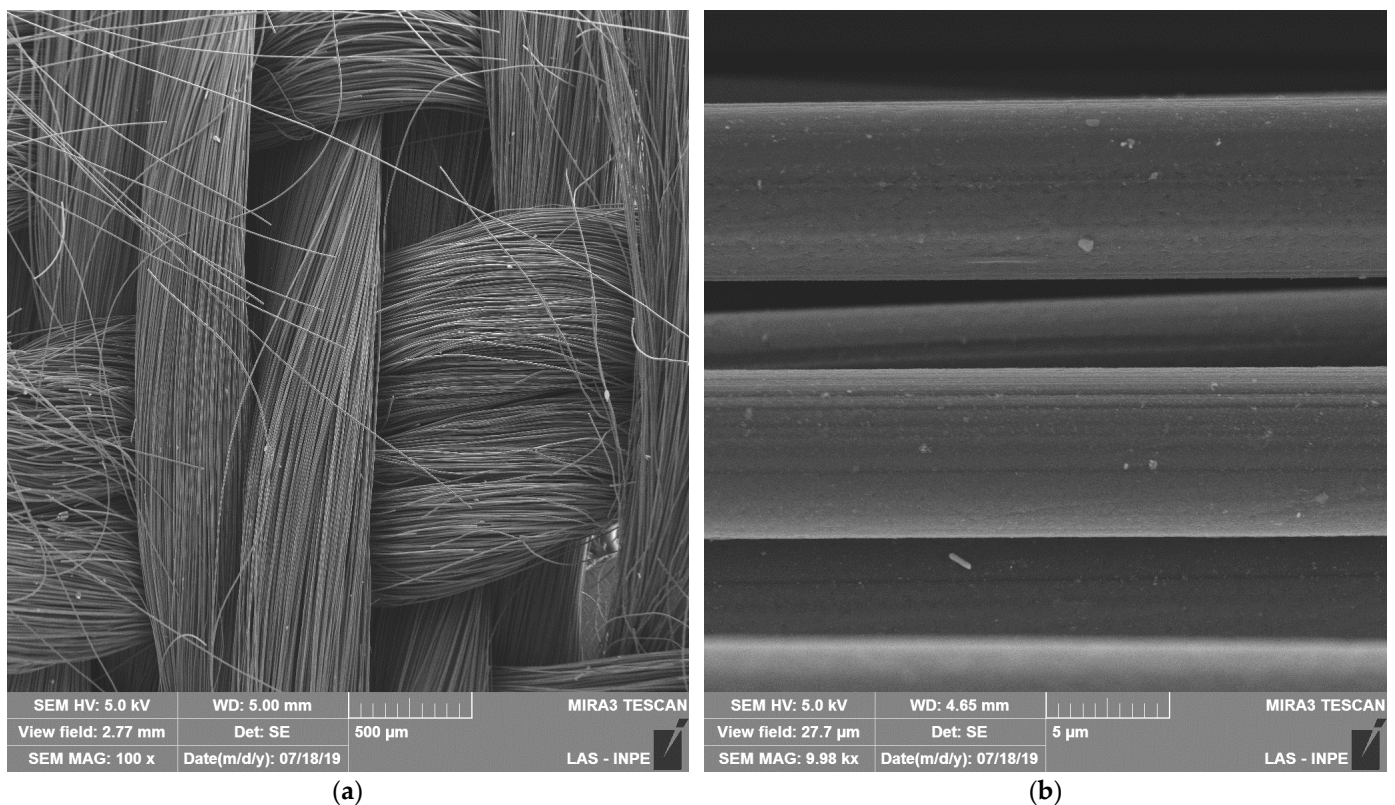


Figure 2. Cont.

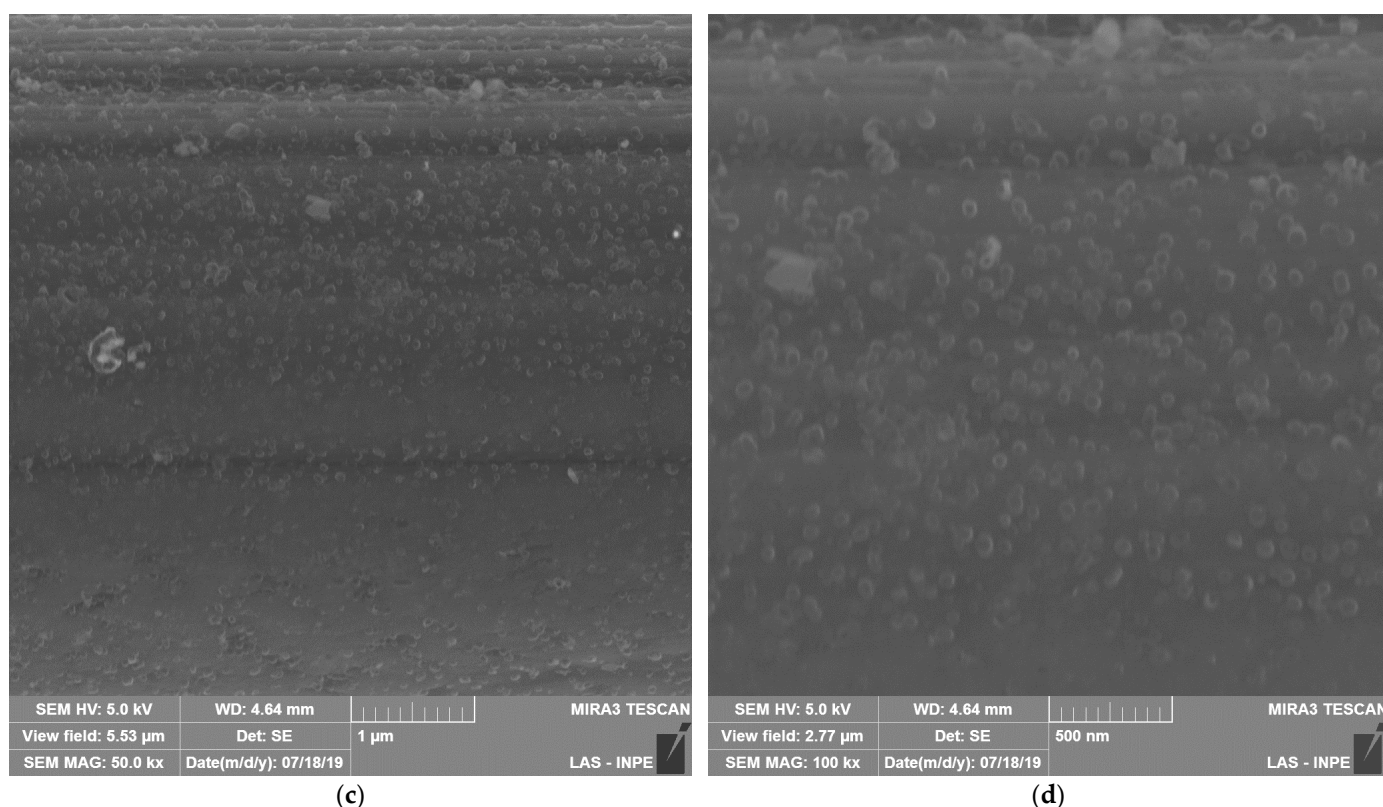


Figure 2. FESEM images of the uncoated CFF. The following magnifications are presented: (a) 100×, (b) 10k×, (c) 50k×, and (d) 100k×.

Following the ALD process, the Al_xO_y -coated CFF was examined under various FESEM magnifications to observe the morphological transformations resulting from the coating application. The sequence of FESEM images obtained at 100×, 10k×, 50k×, and 100k× magnifications after coating (Figure 3) showcased the Al_xO_y film's gradual coverage over the CF surface. At 100× magnification, the CFs preserved their overall structure, with the coating subtly enveloping them. Increasing magnification levels revealed the Al_xO_y film's consistency and comprehensive coverage. At 10 k×, the coating's smoothness and uniformity were apparent, whereas at higher magnifications of 50k× and 100k×, the granular texture of the Al_xO_y film became more pronounced, highlighting its nanoscale film development.

FESEM was employed to assess the morphological transformations of CFFs at various stages of ALD cycle progression, specifically at 1000, 2000, 3000, 4000, and 5000 cycles. The following detailed observations provide a clearer understanding of how the film's morphology evolves with each stage:

- At 1000 cycles, the initial formation of Al_xO_y grains is noticeable. These grains are sparse and primarily nucleate at fiber intersections, where the highest local surface area exists. Initial FESEM observations reveal that the film follows the initial morphology of CFF, increasing grain size and reducing grooves as the technique promotes uniform growth across the entire fiber surface.
- By 2000 cycles, these grains grow larger and begin to coalesce, covering more of the fiber surfaces and reducing the visibility of the underlying fiber texture. FESEM images capture the point where individual Al_xO_y grains begin to touch and coalesce, forming a continuous structure. The granular texture becomes increasingly evident, indicative of a transition from discrete particles to a granular film morphology.
- At 3000 cycles, a continuous and more uniform layer is evident, with significant coverage over the entire fiber structure. This marks a transition from discrete grains to a more homogeneous film.

- By 4000 cycles, the Al_xO_y coating thickens and starts filling the inter-fiber spaces, further enhancing the uniformity of the film across the fabric. This increase in granularity correlates with the volumetric growth observed in the CFF substrate.
- At 5000 cycles, the surface displays a continuous and more porous Al_xO_y film encapsulating the fibers, representing an almost complete morphological transformation compared to the uncoated state. The granular phase precedes the establishment of a totally continuous film, characterized by a larger diameter and a more homogeneous distribution of grains.

FESEM images at $50k\times$ and $100k\times$ magnifications after each stage reveal distinct granularity that signifies the growth stages of Al_xO_y films through the ALD technique. Detailed micrographs trace the morphology from sparse cores to a dense film, offering a visual understanding of the ALD process's ability to control film growth on complex substrates.

The increase in mass of the Al_xO_y film is not merely the result of layer stacking but also from the lateral growth and interconnection of grains, a phenomenon that contributes to the higher volume per cycle calculated for the CFF substrate compared to the flat Si(100) substrate. This is due to the porous and highly rough nature of CFFs, which offers an expansive set of nucleation sites, leading to more pronounced three-dimensional film growth. This dual process of linear growth and volumetric expansion through grain interconnection is facilitated by the complex microstructure of CFF, particularly evident in cycles above 1000.

Through careful documentation and analysis, the ALD process is shown to skillfully capitalize on this microstructural complexity to incrementally increase film thickness and mass, as visually and quantitatively reflected in the FESEM images and growth data.

Figure 4 presents a compelling EDS mapping analysis of Al_xO_y -coated CFFs after undergoing 1000 and 3000 ALD cycles. This figure is instrumental in illustrating the elemental composition of the Al_xO_y thin film and the deposition uniformity imparted by the ALD process over the substrate surface. The EDS maps after 1000 and 3000 cycles of ALD show a clear increase in the coverage and uniformity of the Al_xO_y coating on CFF. This trend suggests that with more cycles, the ALD process continues to deposit thin, conformal layers, improving the uniformity of the coating, which is essential for ensuring the enhanced properties of the CFF are uniformly applied.

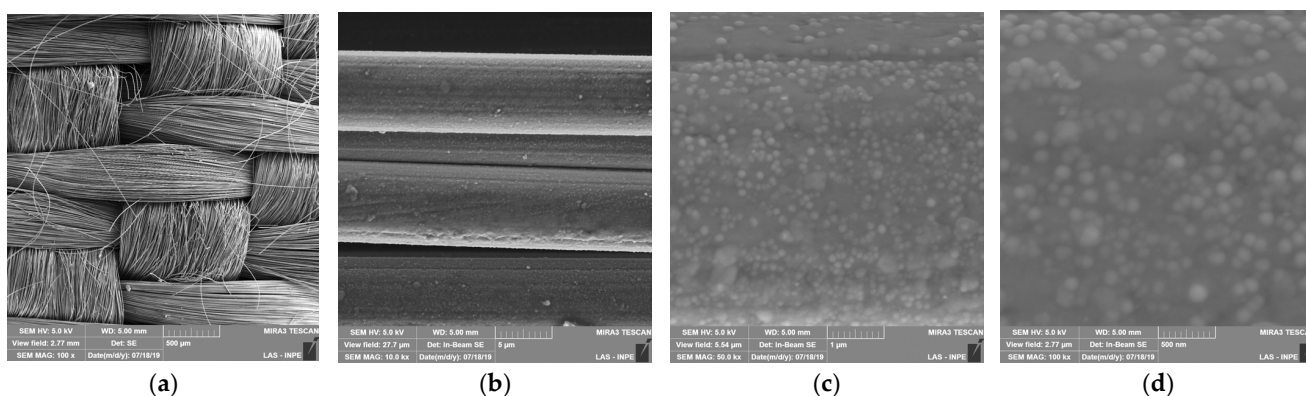


Figure 3. Cont.

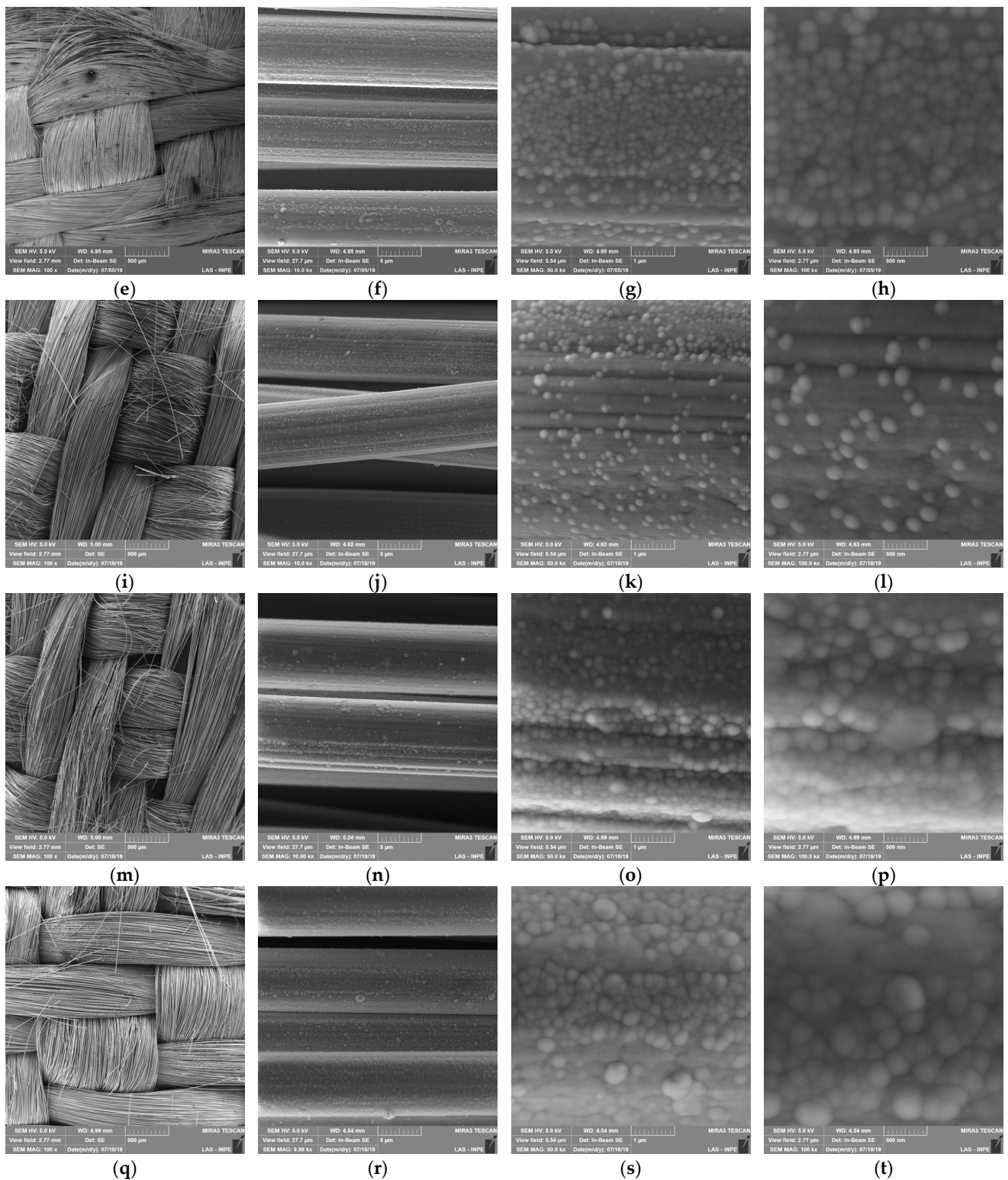


Figure 3. FESEM images of ALD Al_xO_y thin films developed over 1000, 2000, 3000, 4000, and 5000 cycles. The images are organized by magnification levels as follows: (a,e,i,m,q) at 100 \times , (b,f,j,n,r) at 10k \times , (c,g,k,o,s) at 50k \times , and (d,h,l,p,t) at 100k \times , corresponding to the increasing number of cycles, respectively. (a–d)—1000 cycles, (e–h)—2000 cycles, (i–l)—3000 cycles, (n–p)—4000 cycles, (q–t)—5000 cycles.

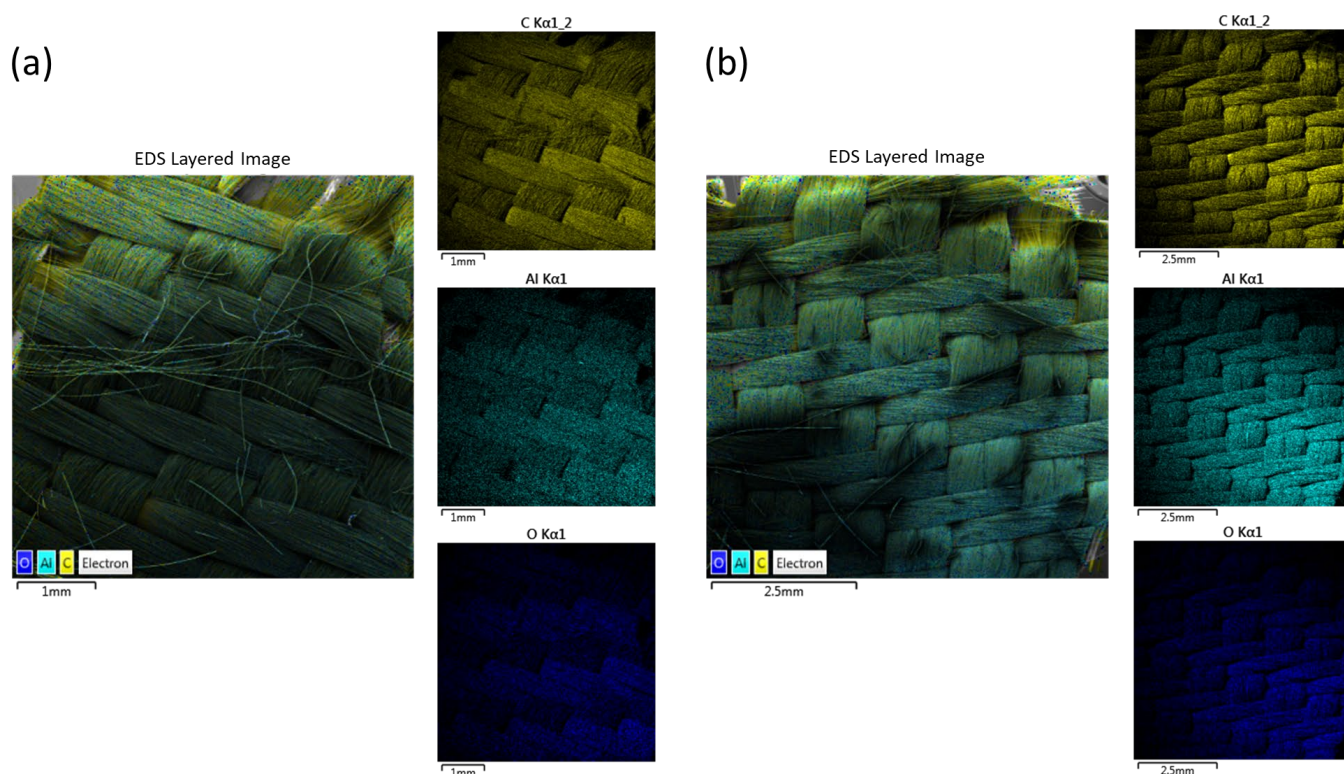


Figure 4. EDS mapping of the Al_xO_y -coated CCF samples for different conditions: (a) 1000 cycles and (b) 3000 cycles.

Table 1 presents the elemental composition analysis obtained by EDS that delineates the gradational changes in the weight percentage (Wt%) of carbon (C), oxygen (O), and aluminum (Al) in both pristine CFF and Al_xO_y -coated CFFs over a range of ALD cycles.

Table 1. Elemental composition obtained by EDS of the pristine CFF and Al_xO_y -coated CFFs. The numbers of 1000 to 5000 are relative to the ALD cycle number.

Element	Pristine CFF	Elemental Composition (Wt%)				
		1000	2000	3000	4000	5000
C	97.3	69.7	40.0	30.7	20.1	12.1
O	2.7	18.3	31.7	34.4	38.6	40.1
Al	0	12.0	28.3	34.9	41.3	47.8

Initially, the pristine CFF reflects its carbon constitution with a weight percentage of 97.3 Wt% for carbon, with minimal oxygen presence. The onset of the ALD process is marked by a discernible shift in elemental composition. By 1000 cycles, the decrease in carbon content decreases to 69.7 Wt% and the oxygen and aluminum contents increase to 18.3 Wt% and 12.0 Wt%, respectively. As the ALD cycle number escalates, we witness a further decline in carbon percentage and an escalation in oxygen and aluminum weights, signaling the progressive build-up of the Al_xO_y layer. Notably, by 5000 cycles, the decrease in carbon to 12.1 Wt% and the rise in aluminum to 47.8 Wt% are indicative of a substantial Al_xO_y deposition.

The Al/O ratio at each stage of the ALD cycle is a critical indicator of the ALD reaction's efficiency and the stoichiometry of the resulting Al_xO_y layer. For Al_2O_3 , the stoichiometric ratio of Al to O should be 1:1.5. Deviations from this ideal ratio can be indicative of various phenomena in the ALD process. An elevated oxygen content compared to aluminum might suggest an excess of oxygen in the reaction environment, possibly

due to more complete oxidation or even the physical adsorption of oxygen molecules on the surface. On the other hand, an Al/O ratio that leans towards aluminum could imply sub-stoichiometric oxidation, potentially leading to a coating with a surplus of aluminum or an incomplete reaction of the aluminum precursor.

By 5000 cycles, the expected stoichiometric balance between aluminum and oxygen would suggest a mature Al_2O_3 coating process. However, the data show an Al/O weight ratio that progresses from 1:1.52 at 1000 cycles to nearly 1:0.84 at 5000 cycles. This suggests that as the number of cycles increases, the ALD process may be depositing relatively more aluminum, possibly due to a saturation of the reaction sites or a change in reaction kinetics leading to a deviation from the expected stoichiometry.

Figure 5 illustrates the FTIR spectra for uncoated and Al_xO_y -coated CFFs across various stages of the ALD process, from 1000 to 5000 cycles. The uncoated CFF spectrum, depicted in black, serves as a benchmark, exhibiting the lowest transmittance percentages and thereby the highest absorption across the measured wavenumber spectrum. This suggests that the uncoated CFFs absorb more infrared radiation, particularly in specific wavenumber bands, as compared to their Al_xO_y -coated counterparts.

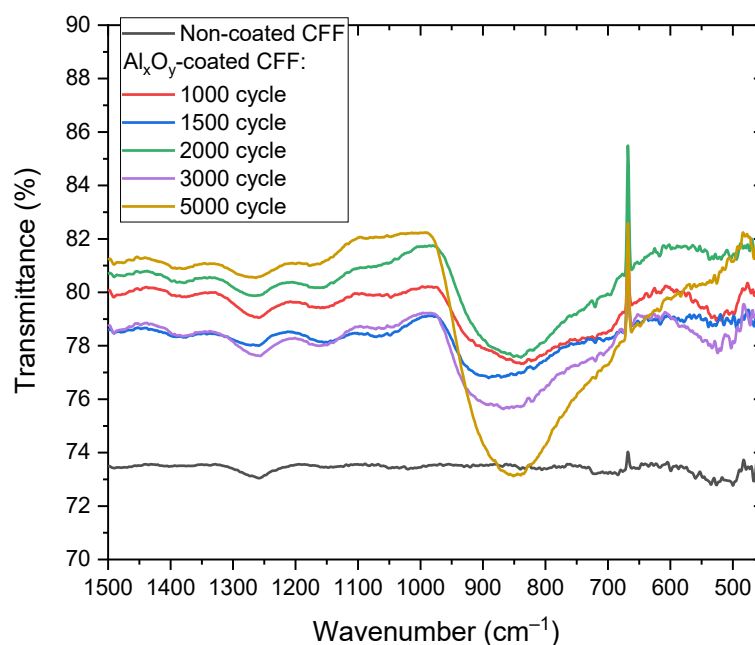


Figure 5. FTIR spectra of the pristine CFF and ALD Al_xO_y -coated CFFs for the reaction cycle number range of 1000 to 5000.

The spectral profiles of Al_xO_y -coated CFFs demonstrate distinct absorption characteristics, with a prominent band evident from 400 to 1000 cm^{-1} . This band corresponds to the vibrations of Al–O bonds that are quintessential of aluminum oxide’s molecular structure. Notably, the band at roughly 516 cm^{-1} can be associated with the vibrational modes of Al–O in the AlO_6 structural units [27]. The absorption feature present near 668 cm^{-1} is predominantly linked to the bending vibrations of O–Al–O bonds [28]. Additionally, the spectra show an absorption band centered in the proximity of 900 cm^{-1} , which is representative of symmetric Al–O stretching vibrations [29].

These spectra highlight the nuanced changes in infrared transmittance as a function of ALD processing, reiterating the complexity introduced by coating CFFs with Al_xO_y and the subsequent alteration in their infrared absorption properties.

Figure 6 presents the Raman spectra of both uncoated and Al_xO_y -coated CFFs subjected to ALD cycles ranging from 1000 to 5000. The analysis spans a spectral range from 50 to 3000 cm^{-1} , revealing key Raman bands characteristic of the CFF substrate. Specifically, the D band, observed at approximately 1337 cm^{-1} , indicates disordered carbon structures,

while the G band at around 1585 cm^{-1} is associated with the graphitic carbon typically found in crystalline forms and is linked to a doubly degenerate deformation mode [30]. Additionally, the spectra include the 2D band near 2700 cm^{-1} and the D + G band around 2900 cm^{-1} . The 2D band is crucial for evaluating the potential layering of graphene-like materials, and the D + G band suggests the occurrence of defect-related interactions within the carbon matrix [30].

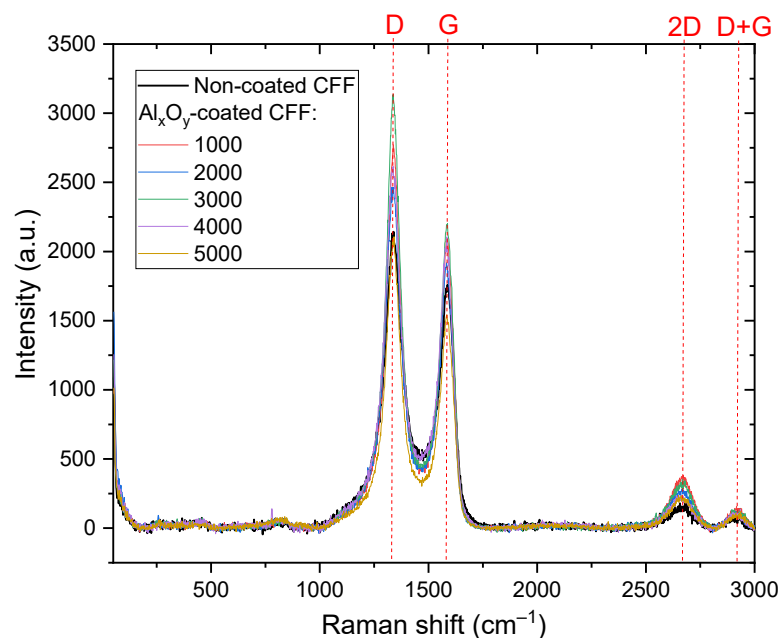


Figure 6. Raman spectra of the uncoated CFF and ALD Al_xO_y -coated CFFs for the reaction cycle number range of 1000 to 5000.

Despite the application of the Al_xO_y coating, these characteristic peaks persist consistently across all treated samples, indicating that the Al_xO_y coating remains amorphous. This amorphous nature of the Al_xO_y coating aligns with the expected behavior of ALD-deposited alumina under the experimental conditions used [12]. The consistent detection of both the 2D and D + G bands alongside the fundamental D and G bands underscores the minimal impact of the amorphous Al_xO_y coating on the carbon substrate's integral structure. The stability of these spectral features across varying ALD cycles highlights the coating's effectiveness in enhancing certain properties without altering the core carbon architecture.

3.3. Chromatic Transformation and Optical Characterization of ALD Al_xO_y -Coated CFFs

Figure 7 exhibits the chromaticity values in the CIE Lab* color space for CFFs coated with Al_xO_y films, revealing the impact of different ALD cycle numbers on the structural colors of the fabrics. The figure captures the vibrant transformation of the CFFs' color as a function of the number of ALD cycles applied, with the colors ranging from green at 1000 cycles to red at 2000 and 4000 cycles, and then shifting to blue at 3000 and 5000 cycles. These colors are derived from chromaticity values extracted from the reflectance spectra based on standards set by the Commission Internationale de l'Éclairage (CIE) [31], providing a precise measurement of the color changes induced by the ALD process.

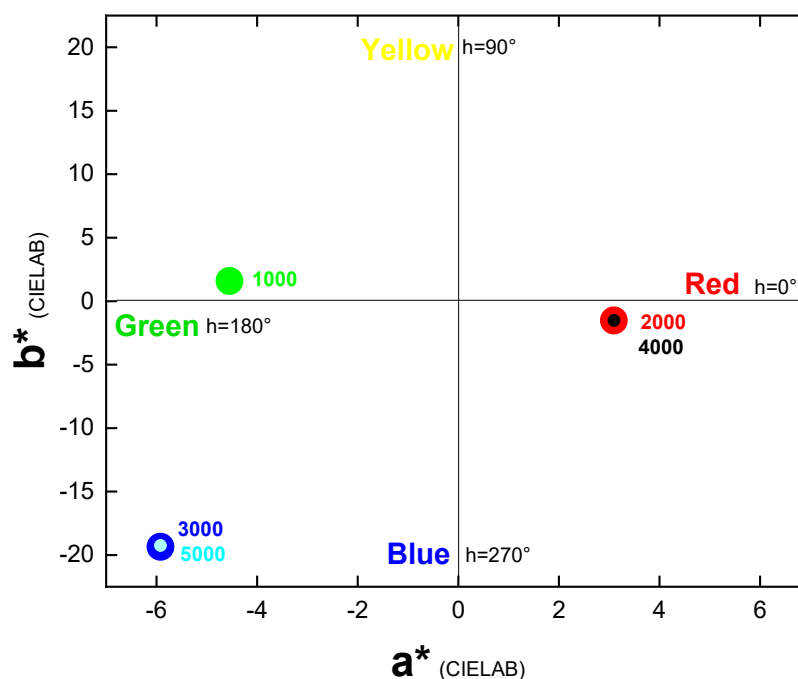


Figure 7. Chromaticity values of CFFs coated with Al_xO_y films after different numbers of ALD cycles, plotted in the CIE Lab* color space.

The color change phenomenon demonstrated in the CFFs is a direct consequence of the structural variations in the Al_xO_y films' thicknesses, which alter the light interference effects and hence the color appearance [6]. This detailed color analysis underscores the potential of ALD to fine-tune the aesthetic attributes of CFFs through controlled film deposition, enabling the customization of fabric colors for diverse applications while maintaining the material's structural integrity and enhancing its functional properties.

Table 2 provides a detailed account of the optical properties of CFF samples coated with Al_xO_y films through varying ALD cycle numbers. The delta (Δ) values indicate the difference in lightness (L^*), chroma (C^*), and hue angle (H^*) compared to the standard uncoated CFF. For chroma, indicated by ΔC^* , positive values across all samples demonstrate an increase in color purity compared to the standard. Notably, the samples subjected to 3000 and 5000 cycles exhibited the most significant deviation from the central L^* axis, implying a pronounced shift in color intensity. Regarding lightness, all samples displayed positive ΔL^* values, signifying a lighter appearance than the standard dark CFF. This lightening effect is consistent with the introduction of the Al_xO_y coating, which influences the fabric's reflectance properties. The hue angle difference, ΔH^* , quantifies the shift in hue compared to the standard CFF. Samples from the 2000- and 4000-cycle treatments remained closest to the hue of the uncoated fabric, suggesting a minimal alteration in color perception. Conversely, samples from 3000 and 5000 cycles showed the largest deviation in hue angle, indicating a more noticeable color shift due to the ALD process.

Table 2. Optical properties (ΔL^* , Δa^* , Δb^* , Δc^* , and ΔH^*) of the CFF samples coated with Al_xO_y films for different reaction cycle numbers.

ALD Cycle Number	ΔL^*	Δa^*	Δb^*	Δc^*	ΔH^*
1000	112.2	108.3	91.5	103.0	102.7
2000	205.9	200.5	185.2	215.9	211.1
3000	280.6	381.3	376.1	310.4	270.1
4000	250.6	482.3	443.7	391.5	412.8
5000	500.0	514.8	511.4	503.7	501.5

The color spectrum observed in Al_xO_y -coated CFFs via CIE Lab* color space is intricately connected to the surface morphology alterations through ALD. The FESEM analysis (Figures 2 and 3) discloses that with more ALD cycles, the granularity and homogeneity of the Al_xO_y film are enhanced, affecting the fabric's roughness and, consequently, its optical interactions. An increase in cycles brings a thicker Al_xO_y coating, altering interference patterns and causing the perceived color shifts. For instance, observing a shift towards the blue end of the spectrum often indicates an increase in the thickness of the Al_xO_y coating. This phenomenon is typically associated with the coatings observed at higher ALD cycle counts, where the FESEM analysis reveals a more significant uniformity in grain distribution and a denser film structure. On the contrary, a trend towards the red spectrum can be indicative of films that are potentially thinner or exhibit less consistency in grain coverage across the surface. Conversely, shifts towards the red may indicate thinner or less grain-continuous films. Compared with the results of Liu et al. [6], where the colors observed with the number of ALD cycles (500–3500) followed the order of blue (1500 cycles), yellow (2000 cycles), green (2500 and 3000 cycles), and red (3500), there is a noticeable difference in the evolution of color with film thickness. However, the authors did not analyze the thickness or mass gain of the Al_2O_3 film, a fact that makes it difficult to compare the materials with a view to explaining the differences.

Finally, the color spectrum observed in Al_xO_y -coated CFFs shares a conceptual link with the structural colors of gold nanoparticle systems described by Ma et al. [32], i.e., the size of the particles profoundly affects the scattering and absorption of light, with larger particles exhibiting shifts in resonance peaks and stronger scattering, leading to a spectrum of observed colors from red to purple as particle size increases. Just as the colors in nanoparticle systems are shaped by factors like particle size, volume fraction, and layer thickness, the hues seen in Al_xO_y -coated fabrics result from alterations in film granularity and thickness due to varying ALD cycles. This parallel underscores the broader principle that structural colors are deeply influenced by material geometry and optical interactions, whether in nanoparticle dispersions or thin-film coatings.

3.4. Thermal Analysis of the Al_xO_y -Coated CFF

The thermogravimetric analysis (TGA) of CFF offers comprehensive insights into its thermal stability under elevated temperatures. The comparison includes uncoated CFF and variants with different thicknesses of Al_xO_y applied via ALD. Figure 8a reveals that all samples retain their mass up to approximately 600 °C, indicating substantial inherent thermal stability. This suggests that CFF alone exhibits significant resistance to thermal degradation.

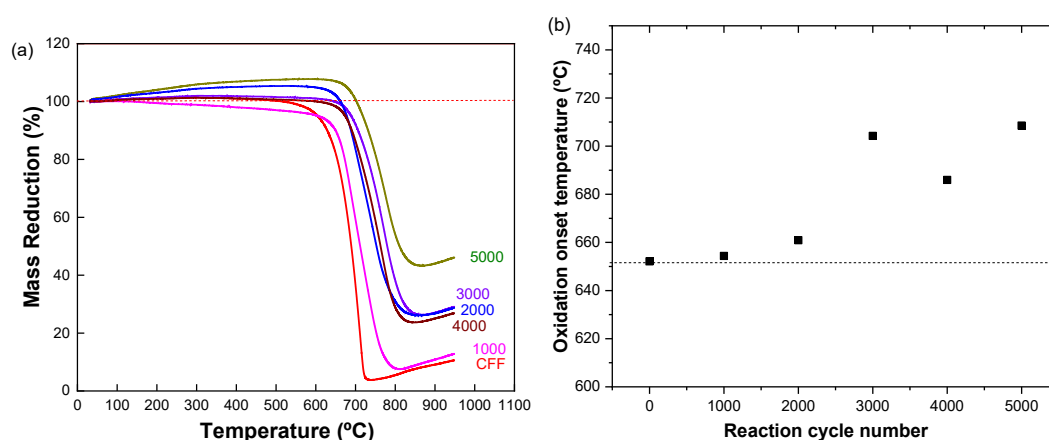


Figure 8. (a) TGA curves of CFF without and with varying ALD-coated Al_xO_y film thicknesses as indicated by deposition cycles. (b) Variation in oxidation onset temperature with respect to ALD cycle number.

At temperatures exceeding 600 °C, the TGA curves display a distinct divergence, where uncoated CFF samples demonstrate a more rapid mass loss in comparison to their Al_xO_y -coated equivalents. This phenomenon accentuates the thermal shielding capabilities of the ALD Al_xO_y coatings, as illustrated in Figure 8b. The figure highlights an upward shift in the oxidation onset temperature with an increasing number of ALD cycles, providing a quantifiable measure of the coatings' effectiveness in boosting oxidation resistance. These observations are consistent with the findings of Dill et al. [19], whose research into ALD-coated carbon and silicon carbide fibers showed that multilayer coatings, including alumina, titania–furfuryl alcohol hybrid, and titanium phosphate, can significantly elevate the temperature at which fiber oxidation commences. Importantly, they underscored the alumina base layer's critical function in offering thermal protection.

Furthermore, the protective performance of these coatings at elevated temperatures is supported by the enhanced fire retardancy detailed in Luo et al.'s study [6]. Their investigation revealed that colored CFFs, when subjected to the direct flame from an alcohol lamp for an extended period of 60 min, managed to maintain their structural integrity. This enhancement in fire resistance strongly complements our study's findings, particularly emphasizing the role of Al_xO_y coatings as a robust thermal barrier, which is notably effective for samples that have undergone 3000 or more ALD cycles. Together, these studies converge on the significant benefit of ALD Al_xO_y coatings in thermally insulating CFFs, underscoring their potential to safeguard materials in high-temperature and oxidative conditions.

Considering the increasing ALD cycles, detailed microstructural analysis using FESEM has demonstrated that as the number of cycles increases, the microstructural changes in the Al_xO_y coatings lead to enhancements in thermal properties. Specifically, as the coatings thicken and become more uniform across the fabric, the ability to resist thermal degradation improves measurably. This shift in thermal properties is directly linked to the microstructural evolution, where denser and more continuous layers provide better thermal insulation and stability.

Figure 8a presents an unusual observation where specific samples, particularly those from 2000, 3000, and 5000 cycles, exhibit mass gain from room temperature to approximately 650 °C. Although such phenomena are rare in TGA analysis, they likely indicate processes like Al_2O_3 oxidation [33] or atmospheric adsorption. The samples with increased ALD cycles, featuring thicker and more continuous Al_xO_y coatings, provide more surface area for these interactions. The oxidation of Al_xO_y at these temperatures may lead to the formation of denser oxides, temporarily increasing the mass. Additionally, the porous structure of the thicker ALD films could adsorb atmospheric gases, further contributing to the observed weight gain.

In contrast, samples with fewer ALD cycles, such as those at 1000 cycles, typically did not show weight gain. These samples likely have thinner coatings with less surface area available for gas adsorption and fewer materials to undergo significant oxidation under the TGA conditions. This variance in behavior underscores the role of microstructural differences in the ALD coatings, influencing their response to thermal conditions. Despite these initial mass gains, all samples ultimately show a significant mass reduction at elevated temperatures, indicating that while Al_xO_y coatings enhance initial thermal stability, they cannot prevent material degradation indefinitely. Future studies will be carried out to better understand this observed phenomenology.

The synthetic air atmosphere, at a flow rate of 50 mL/min during the TGA, likely accelerates oxidation at high temperatures, which the mass loss patterns corroborate. This reactive environment proves challenging for the material's stability, highlighting the complex dynamics between ALD coatings and thermal processes under varying experimental conditions.

Figure 9's differential thermogravimetric (dTG) analysis complements these findings by examining the rate of thermal decomposition. Initially, all dTG curves remain near zero, denoting minimal mass change and thus reflecting strong thermal stability at lower

temperatures. As the temperature climbs, the dTG curves depart from this baseline, marking the onset of decomposition.

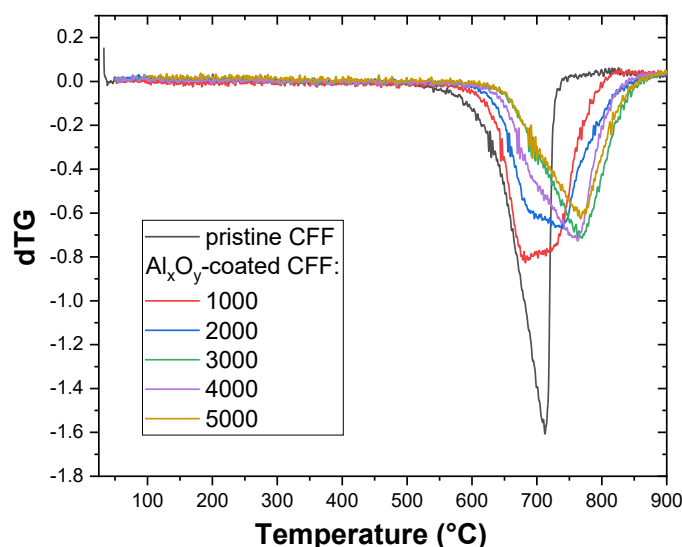


Figure 9. First-derivative curves (dTG) of the uncoated and ALD Al_xO_y -coated CFF samples.

The pristine CFF exhibits a sharp peak in the dTG curves, indicative of rapid mass loss due to oxidation or decomposition. In contrast, Al_xO_y -coated CFF samples demonstrate peaks that incrementally shift to higher temperatures as the ALD cycles increase. This shift is particularly notable for the 5000-cycle sample, signifying a correlation between the number of ALD cycles, the ALD coating thickness, and the resulting enhancement in thermal stability, resulting in a delay of degradation. This shift suggests an increasing onset temperature of decomposition by approximately 60–70 °C, from the uncoated fibers to the highest ALD cycle coated samples, as demonstrated by Dill et al. [19], where ALD-coated fibers showed an increased onset temperature of oxidation from a single layer and only marginal increases with additional layers.

While the TGA data previously hinted at anomalous mass gains, these do not appear as positive peaks in the dTG curves, suggesting that the observed mass gain may be a minor factor in the thermal decomposition process, which is the focus of the dTG.

Overall, the TGA and dTG analyses, in conjunction with the oxidation onset temperatures, present a consistent plot. They confirm the efficacy of ALD Al_xO_y coatings in enhancing CFF's thermal stability, especially noteworthy for high-temperature applications requiring robust thermal resistance. These results underscore the critical role of ALD Al_xO_y in improving the thermal properties of CFF, with the coating's thickness emerging as a pivotal factor in its efficacy.

4. Conclusions

This study showcases the impact of ALD Al_xO_y coatings on CFFs, which are traditionally challenging to dye due to their inherent black color. The methodical application of ALD established a direct correlation between the number of ALD cycles and the resultant increase in the mass of the Al_xO_y films, underscoring the method's consistency and dependability. This consistent increase in mass with additional ALD cycles suggests the potential for tailored thermal management solutions in the aerospace and automotive industries, where precision in material properties is crucial for heat shielding and lightweight structural components.

Although the high conformality of ALD processes, particularly with TMA, is established, our study enriches this understanding by providing detailed quantitative insights into the significantly increased volume of material deposited per cycle when applying ALD to the complex three-dimensional geometries of CFFs. These insights could enhance

the development of next-generation composite materials for high-performance applications in sports equipment and aerospace, where intricate geometries require uniform coating applications.

This quantitative analysis, coupled with comprehensive morphological and functional characterization, underscores the unique efficacy of ALD Al_xO_y coatings in enhancing both the aesthetic and thermal properties of CFFs, demonstrating its potential for specialized applications. The improved aesthetic appeal through controlled coloration processes enables applications in consumer goods where visual design is as valued as functionality, such as in high-end sporting goods and automotive interiors.

Through morphological investigations using FESEM, we unveiled the nuanced micro- and nanoscale structural evolution of the CFF surface attributed to ALD Al_xO_y coating. The morphological evolution, characterized by the coalescence of initially dispersed grains into a dense, continuous layer, plays a pivotal role in both the optical and thermal properties of the coated CFFs. As the grain size increases with more ALD cycles, the Al_xO_y films grow thicker, altering the path of incident light and shifting the reflection spectrum towards the blue end. This granular growth not only contributes to the vivid color spectrum but also enhances the thermal stability of the CFFs, as evidenced by TGA and DTG analyses. The significant reduction in mass loss at elevated temperatures indicates an enhanced resistance to thermal degradation, making ALD Al_xO_y -treated CFFs ideal for use in protective clothing for firefighting and other high-temperature environments where thermal protection is paramount.

The robustness of the Al_xO_y films effectively serves as a thermal barrier, insulating the CFFs and maintaining their structural integrity under high-temperature conditions. This feature opens avenues for novel applications in industries where both aesthetic quality and resilience to high temperatures are crucial, such as in aerospace engine components and automotive heat shields, where maintaining structural integrity at high temperatures is essential for safety and performance.

The comprehensive morphological, optical, and thermal transformation brought about by the ALD Al_xO_y process on CFFs underscores a sophisticated mechanism that intricately ties film growth, grain size evolution, and optical interference effects to the thermal properties of the material. This multifaceted enhancement not only enriches the aesthetic appeal of CFFs but also significantly boosts their thermal resistance, providing robust solutions to current challenges in material engineering and design and opening new avenues for the development of advanced materials in industries requiring high performance under extreme conditions.

Author Contributions: Conceptualization, V.D. and R.P.; methodology, V.D. and R.P.; software, V.D.; validation, V.D.; formal analysis, V.D., N.G., F.M. and R.P.; investigation, V.D., F.M., N.G. and R.P.; resources, H.M. and R.P.; data curation, V.D. and R.P.; writing—original draft preparation, V.D., N.G., G.P., H.M. and R.P.; writing—review and editing, V.D., M.F., H.M. and R.P.; visualization, V.D. and R.P.; supervision, H.M. and R.P.; project administration, H.M. and R.P.; funding acquisition, M.F., G.P. and R.P. All authors have read and agreed to the published version of the manuscript.

Funding: This research was funded by FAPESP, grant number 2018/01265-1, and CNPq, grant numbers 313482/2021-7 and 405637/2022-5. The APC was funded by FAPESP, grant number 2022/03522-7.

Institutional Review Board Statement: Not applicable.

Informed Consent Statement: Not applicable.

Data Availability Statement: Data available upon request.

Conflicts of Interest: The authors declare no conflicts of interest.

References

1. Frank, E.; Steudle, L.M.; Ingildeev, D.; Spörl, J.M.; Buchmeiser, M.R. Carbon Fibers: Precursor systems, processing, structure, and properties. *Angw. Chem. Int. Ed. Engl.* **2014**, *53*, 5262–5298. [[CrossRef](#)] [[PubMed](#)]
2. Frank, E.; Hermanutz, F.; Buchmeiser, M.R. Carbon Fibers: Precursors, manufacturing, and properties. *Macromol. Mater. Eng.* **2012**, *297*, 493–501. [[CrossRef](#)]
3. Hassan, M.F.; Sabri, M.A.; Fazal, H.; Hafeez, A.; Shezad, N.; Hussain, M. Recent trends in activated carbon fibers production from various precursors and applications—A comparative review. *J. Anal. Appl. Pyr.* **2020**, *145*, 104715. [[CrossRef](#)]
4. Kim, J.W.; Lee, J.S. Preparation of carbon fibers from linear low density polyethylene. *Carbon* **2015**, *94*, 524–530. [[CrossRef](#)]
5. Wang, Y.-Q.; Zhou, B.-L.; Wang, Z.-M. Oxidation protection of carbon fibers by coatings. *Carbon* **1995**, *33*, 427–433. [[CrossRef](#)]
6. Luo, Y.; Zhang, Y.; Xing, T.; He, A.; Zhao, S.; Huang, Z.; Liang, Z.; Liu, X.; Liu, Y.; Yu, Y.; et al. Full-Color Tunable and Highly Fire-Retardant Colored Carbon Fibers. *Adv. Fiber Mater.* **2023**, *5*, 1618–1631. [[CrossRef](#)]
7. Khan, M.R.; Kim, H.G.; Park, J.S.; Shin, J.W.; Nguyen, C.T.; Lee, H.-B.-R. Tunable color coating of e-textiles by atomic layer deposition of multilayer TiO₂/Al₂O₃ films. *Langmuir* **2020**, *36*, 2794–2801. [[CrossRef](#)]
8. Zheng, Z.; Wang, H.; Zhao, X.; Zhang, N. Simulation of the effects of structural parameters of glass fiber fabric on the thermal insulation property. *Text. Res. J.* **2018**, *88*, 1954–1964. [[CrossRef](#)]
9. Rodrigues, B.V.M.; Dias, V.M.; Fraga, M.A.; da Silva Sobrinho, A.S.; Lobo, A.O.; Maciel, H.S.; Pessoa, R.S. Atomic layer deposition of TiO₂ thin films on electrospun poly (butylene adipate-co-terephthalate) fibers: Freestanding TiO₂ nanostructures via polymer carbonization. *Mater. Today Proc.* **2019**, *14*, 656–662. [[CrossRef](#)]
10. Ballester, M.F.M.; Doria, A.C.O.C.; Pessoa, R.S.; Rodrigues, B.V.M. Enhancing Microbiostatic Properties of Silicone Catheters with Al₂O₃ Coatings Deposited by Atomic Layer Deposition. *Mater. Lett.* **2023**, *344*, 134400. [[CrossRef](#)]
11. Pessoa, R.S.; Dos Santos, V.P.; Cardoso, S.B.; Doria, A.C.O.C.; Figueira, F.R.; Rodrigues, B.V.M.; Testoni, G.E.; Fraga, M.A.; Marciano, F.R.; Lobo, A.O.; et al. TiO₂ coatings via atomic layer deposition on polyurethane and polydimethylsiloxane substrates: Properties and effects on *C. albicans* growth and inactivation process. *Appl. Surf. Sci.* **2017**, *422*, 73–84. [[CrossRef](#)]
12. Testoni, G.E.; Chiappim, W.; Pessoa, R.S.; Fraga, M.A.; Miyakawa, W.; Sakane, K.K.; Galvão, N.K.A.M.; Vieira, L.; Maciel, H.S. Influence of the Al₂O₃ partial-monolayer number on the crystallization mechanism of TiO₂ in ALD TiO₂/Al₂O₃ nanolaminates and its impact on the material properties. *J. Phys. D Appl. Phys.* **2016**, *49*, 375301. [[CrossRef](#)]
13. Militzer, C.; Dill, P.; Goedel, W.A. Atomic layer deposition onto carbon fiber fabrics. *J. Am. Ceram. Soc.* **2017**, *100*, 5409–5420. [[CrossRef](#)]
14. Hyde, G.K.; Parl, K.J.; Stewart, S.M.; Hinstroza, J.P.; Parsons, G.N. Atomic Layer Deposition of Conformal Inorganic Nanoscale Coatings on Three-Dimensional Natural Fiber Systems: Effect of Surface Topology on Film Growth Characteristics. *Langmuir* **2007**, *23*, 9844–9849. [[CrossRef](#)] [[PubMed](#)]
15. Atasanov, S.E.; Oldham, C.J.; Slusarski, K.A.; Taggart-Scarff, J.; Sherman, S.A.; Senecal, K.J.; Filocamo, S.F.; McAllister, Q.P.; Wetzel, E.D.; Parsons, G.N. Improved cut-resistance of Kevlar using controlled interface reactions during atomic layer deposition of ultrathin (<50 Å) inorganic coatings. *J. Mater. Chem. A* **2014**, *2*, 17371–17379. [[CrossRef](#)]
16. Chen, F.; Yang, H.; Li, K.; Deng, B.; Li, Q.; Liu, X.; Dong, B.; Xiao, X.; Wang, D.; Qin, Y.; et al. Facile and Effective Coloration of Dye-Inert Carbon Fiber Fabrics with Tunable Colors and Excellent Laundering Durability. *ACS Nano* **2017**, *11*, 10330–10336. [[CrossRef](#)]
17. Yang, H.; Yu, Z.; Li, K.; Jiang, L.; Liu, X.; Deng, B.; Chen, F.; Xu, W. Facile and Effective Fabrication of Highly UV-Resistant Silk Fabrics with Excellent Laundering Durability and Thermal and Chemical Stabilities. *ACS Appl. Mater. Interfaces* **2019**, *11*, 27426–27434. [[CrossRef](#)] [[PubMed](#)]
18. Hyde, G.K.; Scarel, G.; Spagnola, J.C.; Peng, Q.; Lee, K.; Gong, B.; Roberts, K.G.; Roth, K.M.; Hanson, C.A.; Devine, C.K.; et al. Atomic Layer Deposition and Abrupt Wetting Transitions on Nonwoven Polypropylene and Woven Cotton Fabrics. *Langmuir* **2010**, *26*, 2550–2558. [[CrossRef](#)]
19. Dill, P.; Pachel, F.; Militzer, C.; Held, A.; Puchas, G.; Knohl, S.; Krenkel, W.; Tegenkamp, C.; Goedel, W.A. Atomic Layer Deposition onto Fabrics of Carbon and Silicon Carbide Fibers: Preparation of Multilayers Comprising Alumina, Titania-Furfuryl Alcohol Hybrid, and Titanium Phosphate. *J. Vac. Sci. Technol. A* **2021**, *39*, 052406. [[CrossRef](#)]
20. Pessoa, R.S.; Pereira, F.P.; Chiappim, W.; Testoni, G.E.; Santos, L.V.; Maciel, H.S. Effect of substrate type on structure of TiO₂ thin film deposited by atomic layer deposition technique. *J. Integr. Circuits Syst.* **2015**, *10*, 38–42. [[CrossRef](#)]
21. Nguyen, C.T.; Cho, E.-H.; Gu, B.; Lee, S.; Kim, H.-S.; Park, J.; Yu, N.-K.; Shin, S.; Shong, B.; Lee, J.Y.; et al. Gradient area-selective deposition for seamless gap-filling in 3D nanostructures through surface chemical reactivity control. *Nat. Commun.* **2022**, *13*, 7597. [[CrossRef](#)]
22. Rontu, V.; Nolvi, A.; Hokkanen, A.; Haeggström, E.; Kassamakov, I.; Franssila, S. Elastic and fracture properties of free-standing amorphous ALD Al₂O₃ thin films measured with bulge test. *Mater. Res. Express* **2018**, *5*, 046411. [[CrossRef](#)]
23. Zhou, Z.; Liu, T.; Khan, A.U.; Liu, G. Block copolymer-based porous carbon fibers. *Sci. Adv.* **2019**, *5*, eaau6852. [[CrossRef](#)]
24. Wilson, C.A.; Grubbs, R.K.; George, S.M. Nucleation and Growth during Al₂O₃ Atomic Layer Deposition on Polymers. *Chem. Mater.* **2005**, *17*, 5625. [[CrossRef](#)]
25. Dilsiz, N.; Wightman, J.P. Surface analysis of unsized and sized carbon fibers. *Carbon* **1999**, *37*, 1105–1114. [[CrossRef](#)]
26. Ruan, R.; Cao, W.; Xu, L. Quantitative characterization of physical structure on carbon fiber surface based on image technique. *Mater. Des.* **2020**, *185*, 108225. [[CrossRef](#)]

27. Gao, M.; Liu, B.; Zhao, P.; Yi, X.; Shen, X.; Xu, Y. Mechanical Strengths and Thermal Properties of Titania-Doped Alumina Aerogels and the Application as High-Temperature Thermal Insulator. *J. Sol-Gel Sci. Technol.* **2019**, *91*, 514–522. [[CrossRef](#)]
28. Chaves, J.; Chiappim, W.; Karnopp, J.; Neto, B.; Leite, D.; da Silva Sobrinho, A.; Pessoa, R. Novel Energetic Co-Reactant for Thermal Oxide Atomic Layer Deposition: The Impact of Plasma-Activated Water on Al₂O₃ Film Growth. *Nanomaterials* **2023**, *13*, 3110. [[CrossRef](#)] [[PubMed](#)]
29. Toledo, R.R.; Santoyo, V.R.; Sánchez, D.M.; Martínez Rosales, M. Effect of aluminum precursor on physicochemical properties of Al₂O₃ by hydrolysis/precipitation method. *Nova Sci.* **2018**, *10*, 83–99. [[CrossRef](#)]
30. Bokobza, L.; Bruneel, J.-L.; Couzi, M. Raman Spectra of Carbon-Based Materials (from Graphite to Carbon Black) and of Some Silicone Composites. *C* **2015**, *1*, 77–94. [[CrossRef](#)]
31. Nascimento, L.; Gasi, F.; Landers, R.; da Silva Sobrinho, A.; Aragão, E.; Fraga, M.; Petraconi, G.; Chiappim, W.; Pessoa, R. Physicochemical Studies on the Surface of Polyamide 6.6 Fabrics Functionalized by DBD Plasmas Operated at Atmospheric and Sub-Atmospheric Pressures. *Polymers* **2020**, *12*, 2128. [[CrossRef](#)] [[PubMed](#)]
32. Ma, L.; Hu, K.; Wang, C.; Yang, J.-Y.; Liu, L. Prediction and Inverse Design of Structural Colors of Nanoparticle Systems via Deep Neural Network. *Nanomaterials* **2021**, *11*, 3339. [[CrossRef](#)] [[PubMed](#)]
33. Ren, L.-F.; Li, Q.-W.; Deng, J.; Yang, X.; Ma, L.; Wang, W.-F. Inhibiting effect of CO₂ on the oxidative combustion thermodynamics of coal. *RSC Adv.* **2019**, *9*, 41126–41134. [[CrossRef](#)] [[PubMed](#)]

Disclaimer/Publisher’s Note: The statements, opinions and data contained in all publications are solely those of the individual author(s) and contributor(s) and not of MDPI and/or the editor(s). MDPI and/or the editor(s) disclaim responsibility for any injury to people or property resulting from any ideas, methods, instructions or products referred to in the content.